Progress In Electromagnetics Research C, Vol. 69, 181–190, 2016

Mechanism of Two Resonant Modes for Highly Resonant Wireless Power Transfer and Specific Absorption Rate

Sangwook Park*

Abstract—In this work, the dosimetry for two resonant modes of a highly resonant wireless power transfer (HR-WPT) system is investigated, and the results are compared. The physical mechanism of the two resonant modes, which occur when the two transmitting and receiving resonators are extremely close to one another, is presented with the simulated results and the equivalent circuit models for the HR-WPT system. The difference between the two resonant modes for the specific absorption rate induced in the head model is discussed by comparing the electromagnetic fields for each mode. Furthermore, the dosimetry for the four-coil HR-WPT system is also investigated under the conditions of a single resonant mode and two resonant modes. The specific absorption rates (SARs) are calculated with head-size and body-size simplified human models at various distances from the WPT system and in each mode. The electric and magnetic fields of the odd mode show stronger distribution than those of the even mode in the area near to the WPT system, while the opposite results are found in the area farther away.

1. INTRODUCTION

Nicola Tesla proposed the concept of wireless power transfer (WPT) in the late 19th century, and he promoted the idea of wireless power distribution for bulbs. The power was delivered through high-frequency AC (Alternating Current) potentials between two plates or nodes [1]. However, the WPT technique was not generally used for power distribution at that time because the power transfer efficiency decreases as distances increase.

An MIT (Massachusetts Institute of Technology) research team proposed using high electromagnetic resonance for the WPT technique [2]. The highly resonant (HR) WPT technique is based on the magnetic induction phenomenon. However, the power transfer efficiency can be increased as much as the high resonance; that is, the high quality factor increases power transfer efficiency at a relatively long distance compared to the magnetic induction technique with a low quality factor. Thus, the technique should use coils, which play a role in resonators with high quality factors. A high quality factor can achieve high efficiency; nevertheless, the power transfer efficiency depending on the resonant frequency is extremely sensitive because the high quality factor represents a narrow bandwidth. Thus, the HR-WPT technique should consider the matching condition to deliver power to loads with high efficiency. One of the considerations related to the technique is that two resonance modes occur at a close distance between the two resonant coils [3]. The two resonance modes represent a split frequency. This phenomenon should also be considered with a view to maintaining high power transfer efficiency.

The HR-WPT technique has attracted attention in many fields and for multiple products. Removal of the power cords of mobile electronic products, such as cell phones and PDAs, represents a natural progression in achieving the ultimate mobility of the product. Applying the WPT technique to electric vehicles (EVs) would also provide advantages, as they would no longer need to be plugged in using

Received 30 August 2016, Accepted 7 November 2016, Scheduled 23 November 2016

* Corresponding author: Sangwook Park (parksw@katech.re.kr).

The author is with the ICT convergence Team, EMI/EMC R&D Center, Reliability & Safety R&D Division, Korea Automotive Technology Institute, Cheoan, Korea.

a power cord, and the battery could be automatically charged after parking the vehicle. In addition, safety advantages in terms of avoiding contact electric shock could also be achieved. Nevertheless, WPT for EVs would require high electrical power — up to hundreds of kilowatts — and larger WPT area, which would also involve increasing electromagnetic field exposure.

Therefore, application of WPT to an EV requires a comprehensive analysis to ensure consumer safety. It is necessary to investigate human safety in relation to the electromagnetic field energies generated from such systems because extremely strong electromagnetic fields are radiated compared to those used in wireless communications. Our focus here is to compare the dosimetry of the two resonant modes in the HR-WPT system. The related foundational studies were conducted in [4–8].

In this paper, the comparison of dosimetry for the two resonant modes is discussed in detail. The physical mechanism of the two resonant modes is described with simulation results and the equivalent circuit models. The simplified HR-WPT system is designed with two resonant coils. The induced electric fields in the anatomically realistic human head model are calculated when the model is exposed to the simplified HR-WPT system. The difference in the magnitude and distribution of SAR for each mode is discussed by comparing the fields for the two modes.

The HR-WPT system, which comprises two feeding loops and two resonant coils, is also designed to evaluate the SAR in the simplified human phantom of the cylindrical model. The electric and magnetic field distributions of the HR-WPT system for each mode are calculated, and their compliance with international guidelines is determined [9–12]. The dosimetry for the HR-WPT system with the simplified human model is assessed at various distances between the model and the WPT system in each mode condition.

2. TWO RESONANT MODES: MECHANISM AND EQUIVALENT CIRCUIT

The WPT system uses the magnetically coupled resonance phenomenon for high energy transfer efficiency at the mid-range distance. In this HR-WPT system, frequency splitting is clearly visible as the distance between the two resonant helix coils decreases [3]. The physical mechanism underlying frequency splitting is that the coupling effect can both enhance and reduce the stored energy. It has been pointed out that frequency splitting in association with two resonance modes can be observed if the coupled resonator circuit is over-coupled, which occurs when the corresponding coupling coefficient is larger than a critical value amounting to 1/Q, where Q is the quality factor of the resonator circuit [13]. It is quite easy to confirm the two split resonant frequencies in our calculated model.

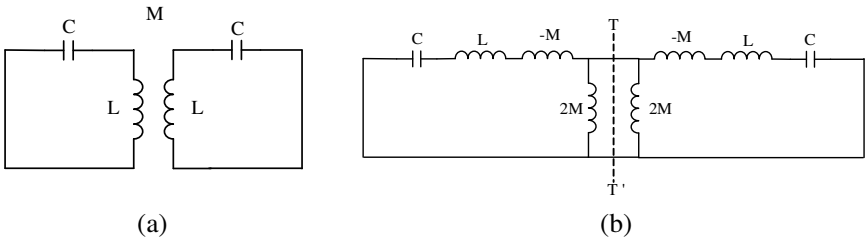

Figure 1. (a) Equivalent circuit of the highly resonant wireless power transfer system exhibiting magnetic coupling (b) an alternative form of the equivalent circuit with an impedance inverter to represent the coupling.

For the fundamental mode near its resonance, an equivalent lumped-element circuit model that does not consider any loss for the coupling structure is illustrated in Figure 1(a), where L and C are the self-inductance and self-capacitance; thus, $1/\sqrt{LC}$ equals the angular resonant frequency of uncoupled resonators and M represents the mutual inductance. According to network theory [14], an alternative form of equivalent circuits in Figure 1(a) can be obtained; this is shown in Figure 1(b). This form yields the same two-port parameters as those of the circuit in Figure 1(a), but it is more convenient for our discussion. Actually, it can be shown that the magnetic coupling between the two resonant helix coils is represent by an impedance inverter $k = \omega M$.

If the symmetry plane T-T' in Figure 1(b) is replaced by a magnetic wall (or an open-circuit), the resultant single resonant circuit has a resonant frequency of

$$f_e = \frac{1}{2\pi\sqrt{(L+M)C}}. \tag{1}$$

The resonant frequency is lower than that of uncoupled single resonator, which is also confirmed in our calculation model. A physical explanation is that the coupling effect increases the stored flux in the single resonator circuit when the magnetic wall is inserted into the symmetrical plane of the coupled structure. Similarly, replacing the symmetrical plane in Figure 1(b) by an electric wall (or a short-circuit) results in a single resonant circuit with a resonant frequency of

$$f_o = \frac{1}{2\pi\sqrt{(L-M)C}}. \tag{2}$$

In this case, the coupling effect reduces the stored flux so that the resonant frequency is increased.

Equations (1) and (2) can be used to find the electric coupling coefficient k as follows:

$$k = \frac{f_o^2 - f_e^2}{f_o^2 + f_e^2} = \frac{M}{L}. \tag{3}$$

This is identical to the definition of the ratio of the coupled magnetic energy to the stored energy of the uncoupled single resonator.

3. DOSIMETRY COMPARISON FOR THE HEAD MODEL

In this section, the dosimetry for the realistic human voxel head model is carried out using the finite-difference time-domain (FDTD) algorithm for even- and odd-mode conditions. The dosimetry computation was performed with the full-wave electromagnetic simulation solver based on the finite integration technique (CST) [15]. The two results are compared and discussed.

A simplified WPT system consisting of two helix coils was designed, as shown in Figure 2. These helix coils play the role of resonators. The source directly feeds at the center of the helix coil (port 1), and the other side (port 2) is terminated with a load of 50 Ω. The helix coils of radii and heights were

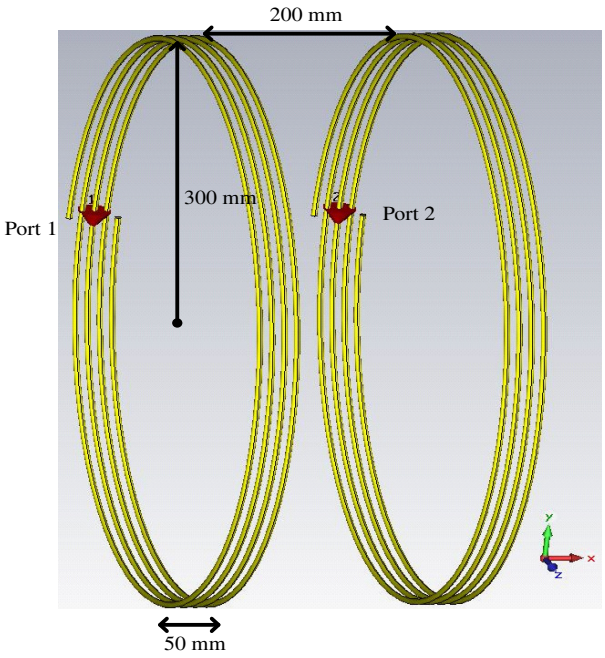

Figure 2. Configuration of the simplified highly resonant wireless power transfer system.

300 mm and 50 mm, respectively, and they each had five turns. The power transfer efficiency ($|S_{21}|^2$) was about 98% at a resonant frequency of 9.72 MHz when the distance between the two helix coils was 330 mm. The resonant frequency was split into the two frequencies of 9.15 MHz and 10.27 MHz, and the power transfer efficiencies were about 94% and 99%, respectively, when the distance between them was 200 mm. In this model, we can find that the power transfer efficiency at higher frequency is larger than that at lower frequency.

Figure 3 shows the magnetic field distributions with the direction of the two helix coil currents at the two resonance frequencies. At the lower resonance frequency (9.15 MHz), the two helix coil currents flow in the same direction, thereby constructing a magnetic wall at the center plane between the two helix coils. This resonant mode is called the "even mode" in this paper. In contrast, at the higher resonance frequency (10.27 MHz), the opposite direction of the two helix coil currents gives rise to constructing an electric wall at the center plane between them. This resonant mode is called the "odd mode" in this paper. The magnetic and electric walls can be seen in the magnetic field distribution of the simplified HR-WPT system, and the equivalent lumped-circuit model can be applied to the description of the physical mechanism of HR-WPT.

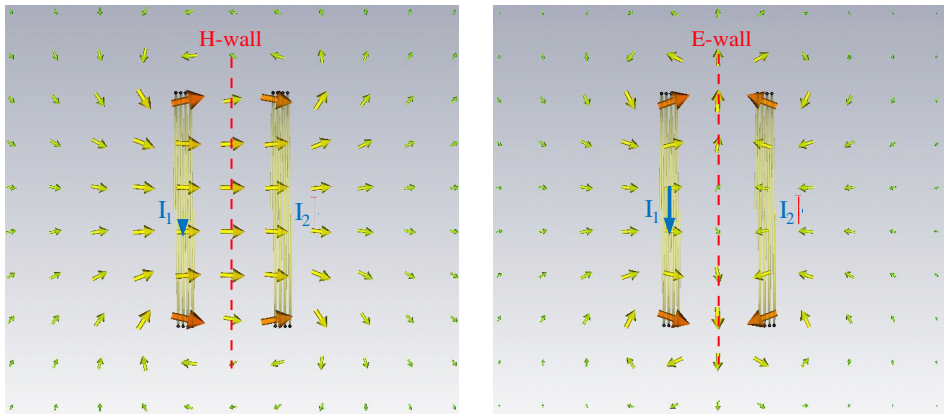

Figure 3. Magnetic field vector distributions with the current direction of the helix coils: (a) even mode (b) odd mode.

Figure 4 shows magnitude distributions of magnetic field strength for the two resonant modes. As can be observed, with the different magnetic field vector distributions for the two resonant modes in the previous section, the magnitudes of the magnetic field strength distribution for the two resonant modes are also different. To compare the electromagnetic field strength for the two resonant modes, spatial distributions for the ratio of electromagnetic field strength of the odd mode to that of the even mode are shown in Figure 5. From the results, we can see that the electromagnetic field strength of the odd mode is stronger than that of the even mode in the area nearest to the two helix coils, which contrasts to the former case in the area far from the two helix coils despite the different power transfer efficiencies of the two resonant modes.

Dosimetry was conducted using CST for each resonant mode of the simplified HR-WPT system. The head part of the Japanese adult male model, TARO [16], was used to compare the two SAR results for each mode. This model, based on accumulated magnetic resonance (MR) images, is composed of 51 tissues and organs with a spatial resolution of 2 mm. The electrical properties of this model were obtained from Gabriel's Cole-Cole models [17]. The SARs were calculated for two cases — a head model situated near the two helix coils (Case 1) and a model situated far away from the two helix coils (Case 2), as shown in Figure 6. The SAR results for the head model are listed in Table 1. All SARs for the odd mode were larger than those for even mode in Case 1, while the reverse was true in Case 2 for both models. These results correspond with the relative field strength of the two resonant modes, as shown in Figure 5. The surface distributions of SAR10g (localized SAR averaged over 10 g of tissue) induced

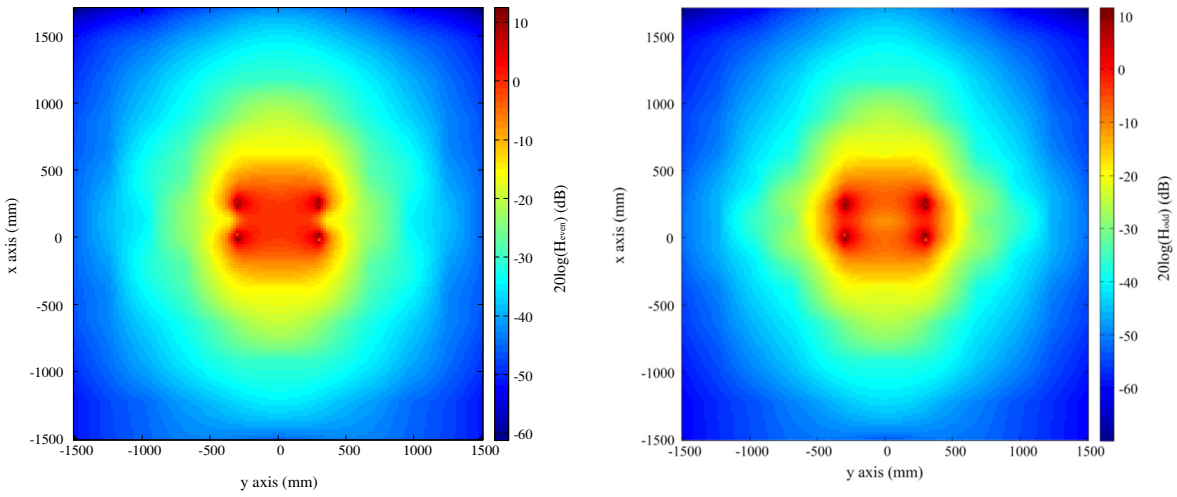

Figure 4. Magnitude distributions of magnetic field strength at (a) lower resonant frequency (even mode) and (b) higher resonant frequency (odd mode).

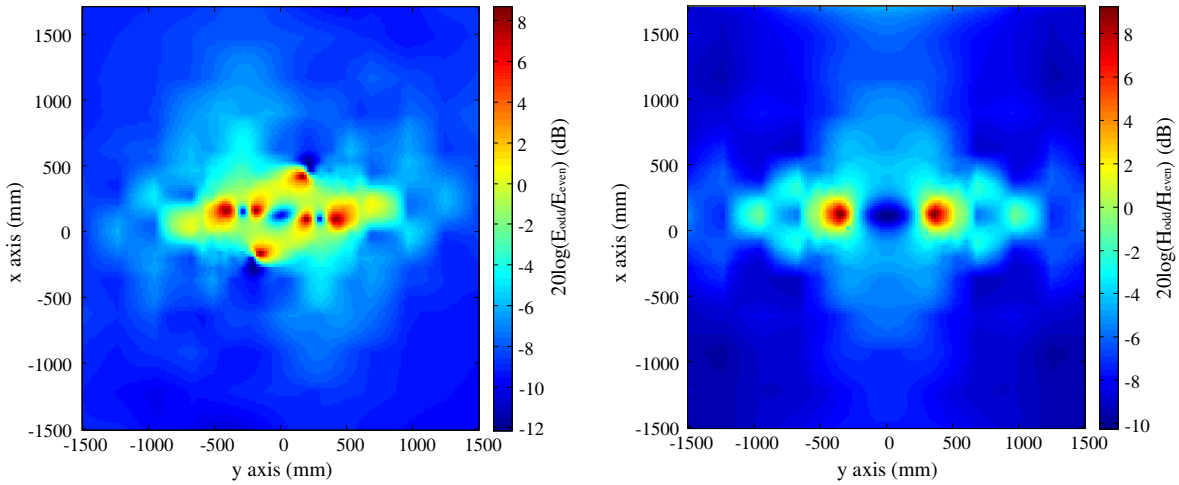

Figure 5. Distributions of the ratio of odd-mode field strength to even-mode field strength: (a) electric field (b) magnetic field.

in the TARO head model for the modes and cases are shown in Figure 7. The same tendency for the magnitude of SARs can also be identified in these results. We see that the distributions for each mode are different in Case 1. This is because the directions and magnitudes of the magnetic field vectors for the two resonant modes are different.

4. DOSIMETRY COMPARISON FOR THE SIMPLIFIED HUMAN PHANTOM

The dosimetry for the realistic human voxel head model was computed using the FDTD algorithm, as described in the previous section. However, computing the dosimetry for the realistic human body model using the FDTD method is time-consuming below approximately 10 MHz. Thus, in this section, the dosimetry for the simplified head-size and body-size phantom models using the electromagnetic commercial solver (FEKO) based on the method of moment (MOM) and finite element method (FEM)

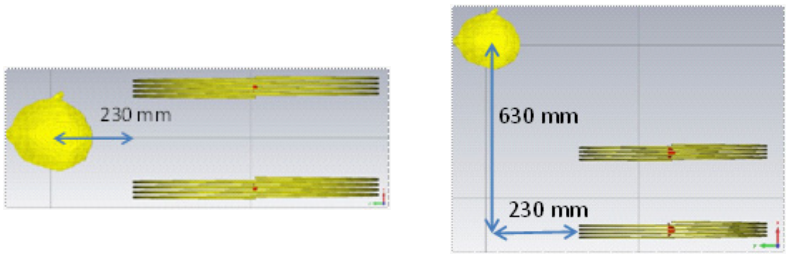

(a) (b)

Figure 6. Position of the calculated model with respect to the WPT system: (a) Case 1 (close to the WPT system). (b) Case 2 (far from the WPT system).

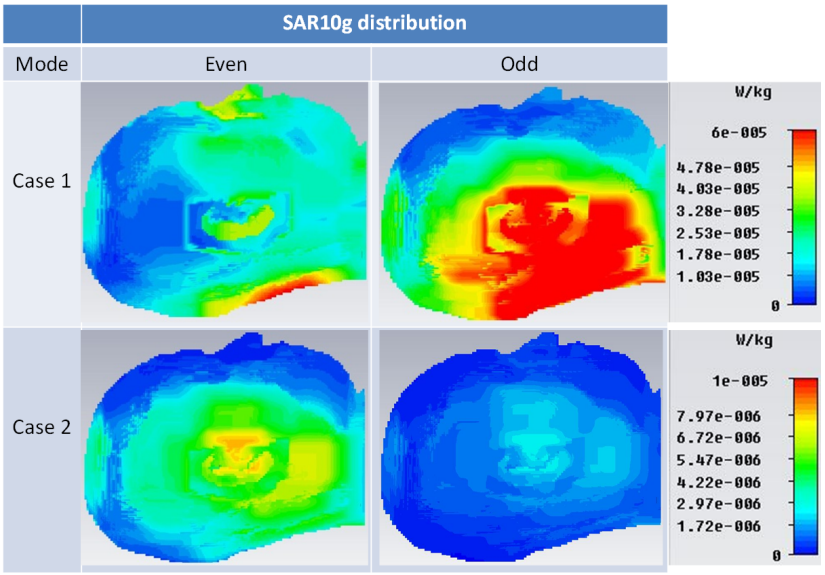

Figure 7. The surface distribution of SAR induced in the TARO head model.

Table 1. Specific absorption rates induced in the TARO head model.

	Case 1		**Case 2**	
Mode	***Even***	***Odd***	***Even***	***Odd***
SAR[1] (μW/kg)	12.9	22.1	2.1	0.7
SAR10 g[2] (μW/kg)	65.7	97.5	14.5	4.1
SAR1 g[3] (μW/kg)	106.5	153.8	21.5	18.4

[1] Whole-head SAR.
[2] Local SAR averaged over 10 g of tissue.
[3] Local SAR averaged over 1 g of tissue.

hybrid technique is described [18]. The field analysis of the HR-WPT system of wire structures is performed by MOM, while the internal electric fields induced in the human phantom of the cylindrical model are calculated using FEM.

The HR-WPT system, composed of two feeding loops and two resonant coils, was designed as shown in Figure 8. The system consists of two resonant coils and two loops placed inside the coils. The coils have five turns and a pitch of 5 mm, and they are used as high-Q resonators. The inner loop

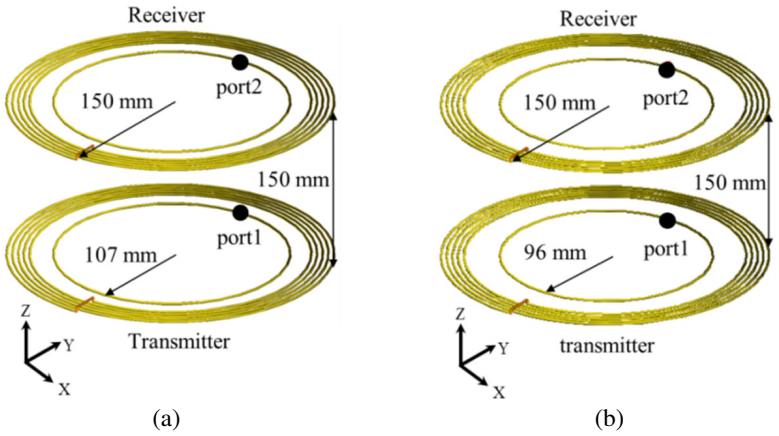

Figure 8. The fourcoil HR-WPT system specification operating in (a) single mode and (b) two resonance modes.

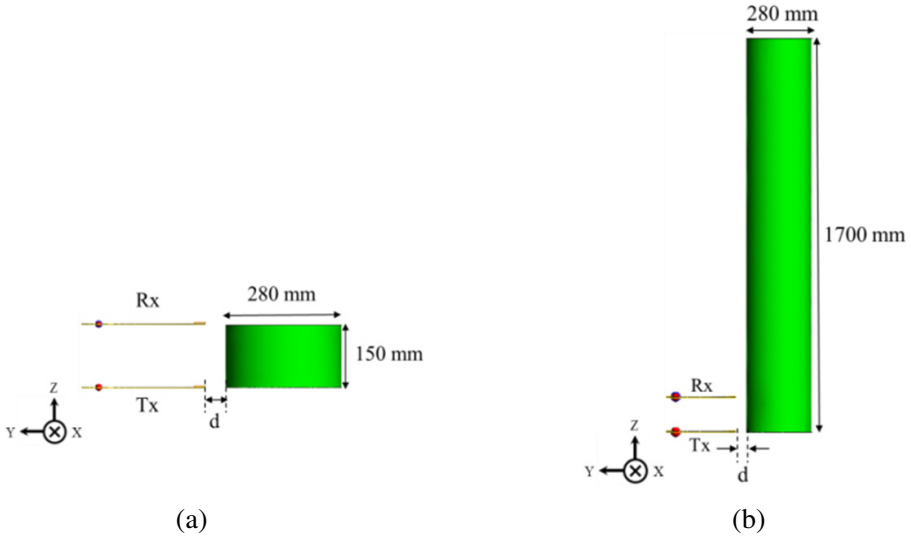

Figure 9. The simplified human phantom of the cylindrical model position with respect to the WPT system: (a) head-sized cylindrical model, (b) body-sized cylindrical model.

plays the role of a matching circuit. The coil radius of the WPT system was designed to be 150 mm, and the power transfer distance was set at 150 mm. Copper wire with a radius of 2 mm was used for the system. The coupling coefficient between the resonant coil and the inner loop changed the input impedance at each port. The matching condition to obtain maximum power transfer efficiency could be achieved by adjusting the size of the inner loop, which was related to the coupling coefficient. In the HR-WPT system, frequency splitting was clearly confirmed as the distance between the two transmitting and receiving resonant coils decreased. However, in the proper coupling coefficient, the two splitting resonant frequencies become a single frequency. In this work, by properly adjusting the size of the inner loop, a single frequency of 13.56 MHz at a loop radius of 107 mm were obtained in the HR-WPT system, as well as the two resonant frequencies of 13.06 MHz and 14.11 MHz at a loop radius of 96 mm, as shown in Figures 8(a) and (b). The two resonant modes at 13.06 MHz and 14.11 MHz represented the even and odd modes, respectively. The power transfer efficiencies for a single (fundamental) mode, even mode, and odd mode were 98.2%, 98.0%, and 96.6%, respectively.

Figure 9 shows the cylindrical model position with respect to the HR-WPT system. The specific absorption rates (SARs) were calculated for each head- and body-size simplified human models at various distances (d) between the HR-WPT system and the simplified human model. The sphere model

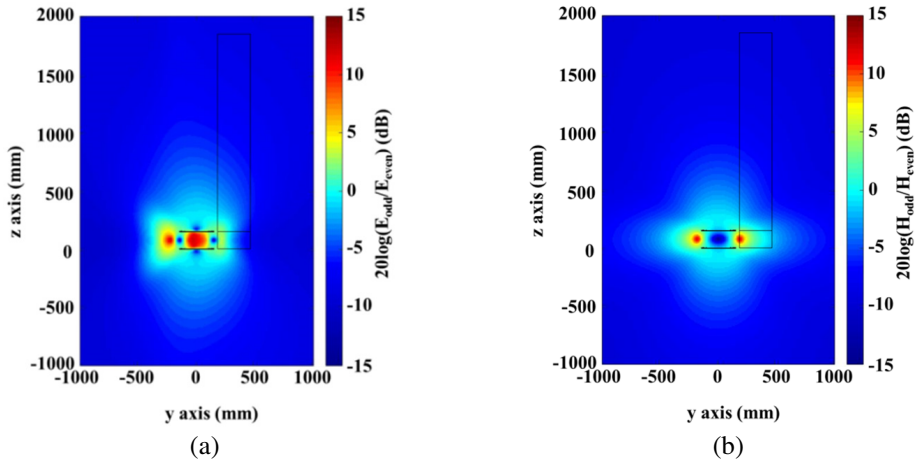

Figure 10. The ratio of the evenmode field intensity to the oddmode field intensity for (a) the electric field (b) the magnetic field.

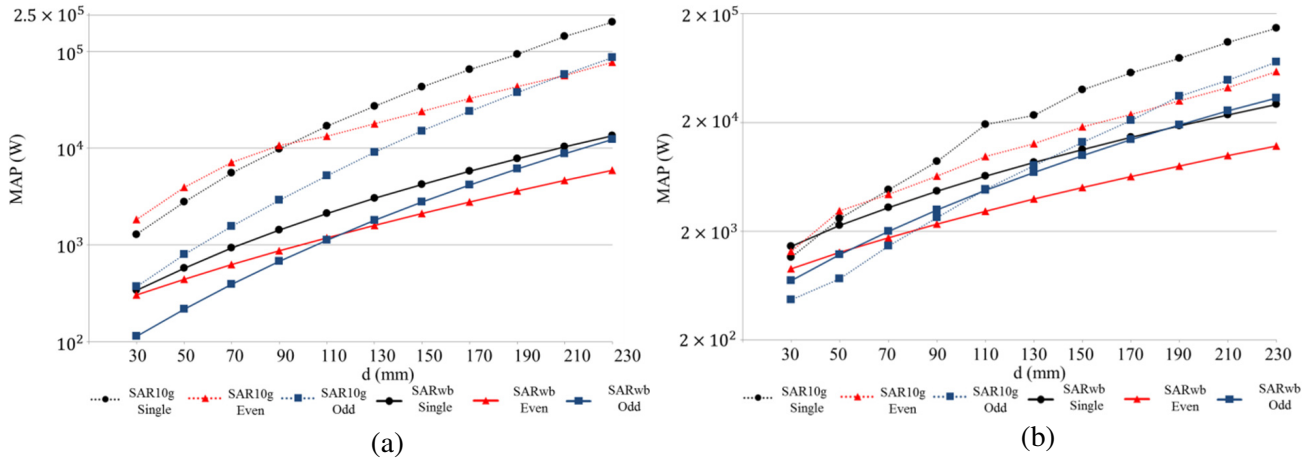

Figure 11. Maximum allowable powers along the distance between the HR-WPT and the human model for (a) the head-sized model and (b) the body-sized model.

was more appropriate compared to the cylindrical shape for the human head. However, to compare two simplified human models with the same distance and exposure shape, the head-size cylindrical model was also chosen. The dielectric properties of the cylindrical model were set to be two-thirds of that of muscle tissue, which represented the average dielectric properties of the human body. The electrical properties of the muscle tissue were taken from Gabriel's Cole-Cole models [8]. The ratio of the odd-mode field intensity to the even-mode field intensity is shown in Figure 10. The results illustrate that the field intensity of the odd mode was stronger than that of even mode in nearest area in the WPT system, while the contrary result was shown in the far area from the WPT system. Thus, the SARs of the even mode were larger than those of the odd mode in the near area from the WPT, while the contrary results were found in the far area from the WPT. The tendency of the previous section was also found in this calculation. The maximum allowable powers (MAPs) referring to the guideline limits could be calculated from the SARs of 1 W of input power. The MAPs for the head-size and body-size human models are shown in Figure 11. As illustrated in Figure 11(b), the MAP results for body-size human model indicated that the single mode and odd mode had advantages in the near and far area, respectively, in relation to the WPT. The lowest MAP, that is, the worst exposure, depended on the mode and distance between the WPT system and the human body. This result suggests that we should consider both localized SAR and whole-body SAR.

5. CONCLUSION — FUTURE WORK

The dosimetry of a highly resonant wireless power transfer (HR-WPT) system was compared for two resonant modes. The physical mechanism of the two modes (even and odd modes) of the HR-WPT system was described. Moreover, it was shown that the difference in the fields for the two resonant modes gave rise to different SARs in the realistic human head model for each resonant mode. Dosimetry was also conducted for the four-coil HR-WPT system when operating in two resonant modes. The SARs were calculated with head-sized and body-sized simplified human models with various distances between the WPT system and the human model to reduce the amount of computation. The field intensity of the odd mode was stronger than that of the even mode in the nearest area to the HR-WPT, while the contrary result was found in the far area from the system. The worst exposure scenario was found at the localized SAR of the odd mode in the nearest area and the whole-body SAR of the even mode in the area far from the WPT system. The MAP results suggested that we should consider both the localized SAR and the whole-body SAR. In future works, the dosimetry will be conducted with a precise whole-body voxel human model based on anatomical structures.

ACKNOWLEDGMENT

This work was supported by a "Development of induction/magnetic resonance type 6.6 kW, 90% EV wireless charger (No. 10052912)" grant from the Ministry of Trade, Industry and Energy of Korea.

REFERENCES

1. Tesla, N. "Apparatus for transmitting electrical energy," US patent number 1,119,732, 1914.
2. Kurs, A. K., A. Moffatt, R. Joannopoulos, J. D. Fisher, P., and M. Soljacic, "Wireless power transfer via strongly coupled magnetic resonances," *Science*, Vol. 317, No. 5834, 83–86, 2007.
3. Sample, A. P., D. A. Meyer, and J. R. Smith, "Analysis, experimental results, and range adaptation of magnetically coupled resonators for wireless power transfer," *IEEE Trans. Ind. Electron.*, Vol. 58, No. 2, 544–554, 2011.
4. Hirayama, H., T. Ozawa, Y. Hiraiwa, N. Kikuma, and K. Sakakibara, "A consideration of electromagnetic-resonant coupling mode in wireless power transmission," *IEICE Elec. Exp.*, Vol. 6, No. 19, 1421–1425, 2009.
5. Sekine, D. and M. Taki, "Relationship between human exposure and resonance mode of wireless power transfer with magnetic resonance," *IEICE Conf.*, B-4-8, 2012 (Japanese).
6. Hirata, A., F. Ito, and I. Laakso, "Confirmation of quasi-static approximation in SAR evaluation for a wireless power transfer system," *Phys. Med. Biol.*, Vol. 58, N241–N249, 2013.
7. Park, S., K. Wake, and S. Watanabe, "Incident electric field effect and numerical dosimetry for a wireless power transfer system using magnetically coupled resonances," *IEEE Trans. Microw. Theory Tech.*, Vol. 61, No. 9, 3461–3469, 2013.
8. Park, S., "Dosimetry for resonance-based wireless power transfer charging of electric vehicles," *J. Electromagn. Eng. Sci*, Vol. 15, No. 3, 129–133, 2015.
9. ICNIRP, "Guidelines for limiting exposure to time-varying electric, magnetic, and electromagnetic fields (up to 300 GHz)," *Health Phys.*, Vol. 74, 494–522, 1998.
10. ICNIRP, "Guidelines for limiting exposure to time-varying electric and magnetic fields (1 Hz to 100 kHz)," *Health Phys.*, Vol. 99, 818–836, 2010.
11. IEEE, "Standard for safety levels with respect to human exposure to electromagnetic fields, 0–3 kHz," *IEEE Standard*, C95.6, 2002.
12. IEEE, "Standard for safety levels with respect to human exposure to radiofrequency electromagnetic fields, 3 kHz to 300 GHz," *IEEE Standard*, C95.1, 2005.
13. Bleaney, B. I. and B. Bleaney, *Electricity and Magnetism*, 3rd edition, Oxford Univ. Press, Oxford, 1976.

14. Montgomery, C. G., R. H. Dicke, and E. M. Purcell, *Principles of Microwave Circuits*, McGraw-Hill, New York, 1948.
15. Computer Simulation Technology, Available online: www.cst.com (accessed on August 15, 2016).
16. Nagaoka, T., S. Watanabe, K. Sakurai, E. Kunieda, S. Watanabe, M. Taki, and Y. Yamanaka, "Development of realistic high-resolution whole-body voxel models of Japanese adult males and females of average height and weight, and application of models to radio-frequency electromagnetic field dosimetry," *Phys. Med. Biol.*, Vol. 49, 1–15, 2004.
17. Gabriel, C. and S. Gabriel, "Compilation of the dielectric properties of body tissues at RF and microwave frequencies," Brooks AFB, San Antonio, TX, USA, 2006.
18. FEKO — EM Simulation Software, Available online: www.feko.info (accessed on August 15, 2016).